HHS Public Access

Author manuscript

Cell Chem Biol. Author manuscript; available in PMC 2017 May 19.

Published in final edited form as:

Cell Chem Biol. 2016 May 19; 23(5): 598–607. doi:10.1016/j.chembiol.2016.03.016.

The late endosome and its lipid BMP act as gateways for the efficient cytosolic access of the delivery agent dfTAT and its macromolecular cargos

Alfredo Erazo-Oliveras, **Kristina Najjar**, **Dat Truong**, **Ting-Yi Wang**, **Dakota J. Brock**, **Austin R. Prater**, and **Jean-Philippe Pellois**[*]

Department of Biochemistry and Biophysics, Texas A&M University, College Station, TX 77843

Abstract

Endosomal entrapment is a severely limiting bottleneck in the delivery of biologics into cells. The compound dfTAT was recently found to circumvent this problem by mediating endosomal leakage efficiently and without toxicity. Herein, we report on the mechanism of endosomal escape of this cell-penetrating peptide. By modulating the trafficking of the peptide within the endocytic pathway, we identify late endosomes as the organelles rendered leaky by dfTAT. We establish that dfTAT binds bis(monoacylglycero)phosphate (BMP), a lipid found in late endosomes, and that the peptide causes the fusion and leakage of bilayers containing BMP. Together, these data identify late endosomes as desirable gateways for cell penetration and BMP as a cellular factor that can be exploited for the development of future delivery agents.

Keywords

Endosomal escape; membrane leakage; cellular delivery; late endosomes; figubis(monoacylglycero)phosphate

Introduction

Achieving the delivery of macromolecules into cells is a current goal of many novel therapeutic approaches and biotechnology applications. From a fundamental cell biology point of view, a key challenge is to address how large and hydrophilic molecules can be made to cross membranes without damaging cells. To date, many cellular delivery strategies have attempted to solve this problem by using the endocytic pathway to gain access to the interior of a cell. These strategies include formulations with liposomes or nanoparticles as well as the use of cell penetrating peptides (CPPs) (Dietz and Bδhr, 2004; Gilleron et al.,

[*]Address correspondence to: Jean-Philippe Pellois, Biochemistry and Biophysics Bldg., Room 430, 300 Olsen Blvd, College Station, TX, 77843-2128. Fax: 979-862-4718, ; Email: pellois@tamu.edu.

Author contributions.

A.E.O. and J.-P.P. designed experiments. A.E.O., K.N., D.T. and T.-Y.W generated data. A.E.O. processed data. A.E.O., K.N., D.J.B. and A.R.P. contributed reagents. A.E.O. and J.-P.P. wrote, edited and approved the final manuscript.

2013; Heitz et al., 2009; Iversen et al., 2011; Liu et al., 2013; Perche and Torchilin, 2013). Upon reaching the cell surface, delivery agents and macromolecular cargos can be initially internalized by various endocytic mechanisms (Bechara and Sagan, 2013). Endocytic uptake is followed by endosomal maturation, a process during which the endocytosed material traffics to endocytic organelles that include early endosomes, recycling endosomes, late endosomes or lysosomes (Gruenberg, 2001; Scott et al., 2014). For most delivery applications, this process alone is not useful as the material trapped in the lumen of endocytic organelles is restricted from other cellular compartments. The latter renders the cargo inactive and unable of exerting a biological response. To achieve functional cellular penetration beyond the endocytic pathway (cytosolic penetration), delivery agents need to mediate the transfer of macromolecular cargos to the cytosolic space from the lumen of endocytic vesicles. Such so-called endosomal escape activities have been reported for lipids, lysosomotropic agents, osmolytic compounds, and for CPPs (Eguchi et al., 2009; El-Sayed et al., 2009; Erazo-Oliveras et al., 2012; Gujrati et al., 2014; Lin and Engbersen, 2008; Varkouhi et al., 2011). However, these activities are typically very poor (Lee et al., 2008; Schwarze et al., 2000) and, because it is challenging to elucidate low efficiency processes, not understood on a molecular level. As a result, the development of delivery agents that would circumvent this problem is often limited to a trial and error process with low success rates. In order to unblock this bottleneck, mechanistic insights are urgently needed.

A prototypical CPP is HIV TAT. TAT can escape the endocytic pathway, yet only at a very low efficiency (Gao et al., 2009; Gillmeister et al., 2011; Lee et al., 2010). Recently, we have identified that simply linking multiple copies of the HIV TAT peptide sequence (RKKRRQRRR) can greatly amplify this activity (endosomal escape) (Angeles-Boza et al., 2010; Erazo-Oliveras et al., 2014). For example, dfTAT, a disulfide-bonded dimer of TAT labeled with the fluorophore tetramethylrhodamine (fTAT), displays an unusually high propensity to cause endosomal leakage and primarily localizes in the cytosol and nucleus. This agent delivers cell-impermeable small molecules, peptides and proteins into cells by a simple co-incubation protocol (Erazo-Oliveras et al., 2014). Notably, the leakage of intracellular organelles induced by dfTAT does not cause a reduction in cell viability and proliferation. Remarkably, endosomal leakage leads to a minimal transcriptional response and cells recover from this process within minutes. On one hand, by combining high delivery efficiency and low physiological impact, dfTAT is, in principle, an immediately useful delivery agent for numerous cell-based assays. On the other hand, dfTAT provides a unique tool that can be used to gain mechanistic insights into the endosomal escape process and into the complex interactions taking place between delivery agents and the endocytic pathway.

Herein, our goal is to elucidate where and how dfTAT escapes from the endocytic pathway. We establish that the late endosome is the site of cytosolic penetration and that the phospholipid bis(monoacylglycero)phosphate (BMP) is a cellular factor involved in membrane leakage. Our results identify a new model for cytosolic penetration and provide a mechanistic basis for the rationale design of molecules that can escape the endocytic pathway efficiently and transport hydrophilic molecules across hydrophobic cellular barriers.

Results

dfTAT cytosolic penetration requires trafficking to a specific destination in the endocytic pathway

In order to characterize the membrane-disrupting activity of dfTAT, we first examined the concentration dependence of endosomal escape for dfTAT, using fTAT as a control (Fig. 1a). A pulse-chase experiment was carried out by incubating dfTAT with cells for 5 min to allow for endocytic uptake. Cells were then washed with heparin sulfate to remove extracellular peptide and monitored by fluorescence microscopy as a function of time. In this assay, endosomal retention is apparent as a punctate staining (Fig. 1b, fluorescence images in bottom right panel). In contrast, cytosolic penetration is observable as a diffuse fluorescence as well as a nucleolar staining (Fig. 1b, fluorescence images in top right panel). This is consistent with the nucleolar signal contained in the TAT sequence (Vivès et al., 1997) and demonstrates the intracellular localization of the fluorescence signal detected. At 20 μM, the maximum concentration tested, fTAT showed endosomal entrapment exclusively. Similarly, dfTAT displayed a punctate distribution at 1 μM (Fig. 1b). At 5 μM and above, cells became positive for cytosol and nucleoli staining (the number of cells with positive cytosolic and nucleolar staining are depicted as penetration (+) % in Figure 1b). (Because nucleolar staining presumably happens after cytosolic entry, we use this intracellular fluorescence distribution as indicative of endosomal escape and cytosolic penetration). Notably, the percentage of cells displaying cytosolic penetration increases with time, indicating the progressive escape of the peptide from the endocytic pathway (Fig. 1b). This percentage increased with the concentration of dfTAT (at 20 μM, the maximum concentration tested, dfTAT does not permeabilize the plasma membrane of cells and does not show significant toxicity 1 or 24 h after incubation, Fig. S1 and S2, respectively). Yet, based on the slope of the time series graphs obtained, the kinetics of the process did not vary significantly with concentration, suggesting that a concentration-independent cellular maturation process might be involved. Together, these data indicate that higher peptide accumulation inside endosomes leads to a higher probability of escape. Yet, because of the relatively constant time window required for escape, they also suggest that a biological process is a limiting rate and that the peptide needs to reach a specific destination before escape is allowed.

dfTAT escape is downstream of early endosomes but does not involve lysosomes or retrograde transport to trans-golgi network

In order to identify the endocytic organelles involved in dfTAT escape, the endocytic pathway was blocked at various steps using dominant negative trafficking proteins (Bucci et al., 1995; Mainou and Dermody, 2012; Stenmark et al., 1994; Vonderheit and Helenius, 2005; Zerial and McBride, 2001) or trafficking inhibitors (Nelson et al., 2013; Stechmann et al., 2010) (Fig. 2a). Low concentrations of dfTAT were used to monitor the trafficking of the peptide within the endocytic pathway by fluorescence microscopy. Trafficking inhibitors were then examined for their ability to modulate or inhibit endosomal escape mediated by high concentration of dfTAT. Co-localization experiments with rab5-EGFP (Bucci et al.; Sönnichsen et al., 2000) and rab7-EGFP (Sugaya et al., 2011; Vitelli et al., 1997) showed that dfTAT reaches early and late endosomes after endocytic uptake (condition 1 in Fig. 2b). Overexpression of these proteins does not impair endosomal escape (condition 2 in Fig. 2b

and Fig. 2c). In contrast, overexpression of dominant negative rab5 (rab5(S34N)) or dominant negative rab7 (rab7(T22N)), proteins that disrupt trafficking to early and late endosomes respectively (Bucci et al., 2000; Colpitts et al., 2007; Feng et al., 2001; Li et al., 1994), inhibited endosomal escape (Fig. 2b and c) (this effect is not caused by a decrease in overall endocytic uptake, as assessed by the total fluorescence of cell lysates; Fig. 2c). This indicates that endosomal escape does not take place in early endosomes or vesicles but from an endocytic compartment downstream (*e.g.* late endosomes, recycling endosomes, the trans-golgi network, or lysosomes). dfTAT did not co-localize with FITC-transferrin, a marker of recycling endosomes (Ullrich et al., 1996; Wilson et al., 2000), making escape from this compartment unlikely (Fig. 2d). The retrograde transport inhibitor retro-2 (Nelson et al., 2013; Stechmann et al., 2010), while capable of inhibiting the transport of the trans-golgi network (TGN) marker mEmerald-TGOLN2 (Lengfeld et al., 2012), had no effect on dfTAT-mediated escape (Fig. 2e). Blocking endocytic trafficking from late endosomes to lysosomes is currently not possible. To circumvent this problem, lysosomes were preloaded with the peptide DEAC-k5, where DEAC is a blue fluorophore and k5 is a sequence of D-lysine residues, imparting both endocytic uptake and protease resistance to this peptide (Fig. S3). By itself, DEAC-k5 accumulated in the endocytic pathway and, over time, co-localized with perinuclear organelles stained with LysoTracker® Green (exp 1 and 2 in Fig. 2f), consistent with lysosomes. When dfTAT was added shortly after DEAC-k5 incubation, dfTAT mediated DEAC-k5 cytosolic release (exp 3 in Fig. 2e). This presumably happened because dfTAT is able to reach and disrupt organelles containing DEAC-k5. Conversely, when the period between DEAC-k5 and dfTAT incubation was extended to a point allowing for lysosomal accumulation of DEAC-k5, dfTAT displayed a cytosolic distribution while DEAC-k5 remained punctate (exp 4 in Fig. 2f). These data indicate that dfTAT escapes the endocytic pathway upstream of lysosomes and therefore does not confer lysosomal leakage.

dfTAT interacts with BMP, a lipid enriched in late endosomes, and causes the leakage of liposomes that mimic the lipid composition of these organelles

By excluding organelles that are upstream or downstream in the pathway, the previous assays pinpoint late endosomes as likely sites of endosomal release. The membranes of late endosomes are rich in the negatively-charged phospholipid bis(monoacylglycero)phosphate (BMP) (Kobayashi et al., 1999; Kobayashi et al., 1998; Kobayashi et al., 2001). Interestingly, low efficiency (endosomal escape) monomeric TAT was previously shown to cause leaky fusion of BMP–containing liposomes (Yang et al., 2010). Based on the notion that dfTAT is dramatically more active than TAT *in cellulo*, we hypothesized that dfTAT might disrupt BMP-containing bilayers more effectively than TAT and that this activity might be sufficient to explain endosomal leakage. To test the idea, large unilamellar vesicles (LUVs) with a lipid composition consistent with that of late endosomes were prepared (L.E. LUV composed of BMP:PC:PE,). Liposomes with a plasma membrane or early endosome composition were used as control (E.E./P.M. LUVs composed of PC:PE:Chol,). LUVs were preloaded with the fluorophore calcein to probe for leakage. Both TAT and dfTAT showed a high propensity to form lipid/peptide aggregates with BMP-containing LUVs (L.E. LUVs) (Fig. 3a). These aggregates formed a pellet upon low speed centrifugation. At the peptide:lipid ratio used (1:50), the fraction of peptide associated with the LUV pellet was 100% for both fTAT and dfTAT (as shown in Figure 3b, the affinity of dfTAT for BMP-

containing liposomes is approximately twice that of fTAT). Conversely, dfTAT did not associate with E.E./P.M large multilamellar vesicles (MLVs) (e.i. lacking BMP) (Fig. 3b). After treatment of LUVs with peptide (leakage experiments), the supernatant was purified by gel filtration to establish the presence of free calcein. In the case of fTAT, peptide/LUV aggregation was not accompanied by release of calcein from the lumen of LUVs, regardless of the concentration of peptide tested (Fig. 3a). In contrast, calcein leakage was observed with dfTAT (as indicated by the green colored supernatant in Figure 3a). In particular, a 10 μM solution of dfTAT (P:L of 1:50) caused leakage from BMP-containing LUVs (38% leakage efficiency) but not from LUVs lacking BMP (<5% leakage, Fig. 3a). Given that dfTAT is positively charged (total of 16 positive charges), it is logical that this peptide would electrostatically interact with L.E. LUVs containing the anionic lipid BMP but not with E.E./P.M. LUVs that only contain zwitterionic phospholipids. To address whether dfTAT binding to negatively-charged lipid bilayers is sufficient to induce membrane disruption, leakage assays were performed with LUVs containing phosphatidic acid (PA) and phosphatidylglycerol (PG). Like BMP, PA and PG are anionic phospholipids, the latter being a structural isomer of BMP. LUVs containing PA and PG were treated with dfTAT (10 μM, P:L of 1:50,). Under these conditions, dfTAT was fully bound to LUVs, regardless of whether they contain BMP, PA, or PG (Figure 3c, BMP, PA and PG contain the same 18:1 fatty acids). However, calcein leakage was greatly diminished when PA or PG were used instead of BMP (Figure 3c). These results therefore illustrate that properties other than lipid charge are important for dfTAT-mediated leakage

Because of its overall inverted cone shape, BMP is prone to form inverted micelles and is fusogenic (Chevallier et al., 2008; Hafez et al., 2001; Kobayashi et al., 2002). To examine whether these properties underlie the leakage mediated by dfTAT partitioning experiments between hexanes and water were performed. In this assay, hexanes are used to mimic the hydrophobic environment of a lipid bilayer and lipids are tested for their ability to transfer dfTAT from water to the organic phase via inverted micelle formation (Herce et al., 2014). Our rationale was that this assay might reveal additional differences between dfTAT and fTAT as well as provide insights into how dfTAT interacts with BMP within a bilayer. While dfTAT was soluble in water by itself, partitioning into hexanes was achieved in the presence of BMP at low lipid concentrations (Fig. 3d). In contrast, PC, PA and PG were considerably less effective at promoting the transfer of peptide into the organic phase. fTAT was also transferred into hexanes by BMP. Yet, the concentration of BMP required to achieve phase transfer of 50% of the dfTAT present was approximately 50-fold lower than that required for fTAT. This was observed when the concentration of fTAT was equal to or double that of dfTAT (this was done to account for the fact that one molecule of dfTAT contains two copies of fTAT). Overall, these data highlight a unique relationship between BMP and dfTAT and illustrate that BMP can mediate the insertion or transfer of this peptide into a lipid bilayer. They also mirror the respective endosomolytic activity differences observed between dfTAT and fTAT, providing a plausible model for how endosomal escape is achieved.

An anti-BMP antibody inhibits dfTAT-mediated liposome leakage and fusion *in vitro* and blocks cytosolic penetration and macromolecular delivery *in cellulo*

In order to determine the involvement of BMP in dfTAT-mediated endosomal leakage in a cellular context, we employed an anti-BMP monoclonal antibody (mAb) (Kobayashi et al., 1998; Kobayashi et al., 2001; Le Blanc et al., 2005). Our rationale was that this bivalent antibody might be able to bind BMP and possibly modulate fusion of BMP-containing liposomes. We first examined this possibility in our *in vitro* assay with BMP-containing LUVs. As shown in Figure 4a, anti-BMP mAb inhibited the leakage of L.E. LUVs in a dose dependent manner. Notably, this was achieved without an apparent reduction of dfTAT binding (Fig. 4a) consistent with the notion that anti-BMP mAb can exert an inhibitory effect without preventing dfTAT from interacting with the lipid bilayer. In addition, a control monoclonal antibody not targeting BMP had no effect on LUV leakage. In order to test whether anti-BMP exert its inhibitory effect by blocking liposomes fusion, a lipid-mixing assay was performed. In this assay, L.E. liposomes doped with 10% pyrene-PC were mixed with unlabeled L.E. liposomes. Fusion between these liposomes results in the dilution of pyrene excimers in the bilayer and in a decrease in the fluorescence of these species (pyrene monomers emit at 379 nm while excimers emit at 470 nm). As demonstrated in Figure 4b, dfTAT, but not fTAT, caused a pronounced reduction in fluorescence at 470 nm, indicative of fusion between labeled and unlabeled liposomes. In addition, while anti-IgG mAb had not effect, anti-BMP mAb was able to counteract dfTAT-induced lipid mixing. However, anti-BMP does not appear to completely abolish lipid mixing. This suggests that, while lipid mixing is required for leakage, not all lipid-mixing events might result in leakage. Overall, these results show a direct correlation between leakage and fusion. They also suggest that anti-BMP might prevent dfTAT-induced leakage by binding onto the surface of liposomes and by preventing liposomes from coming into contact with one another.

To test whether similar effects could be observed *in cellulo*, cells were pre-incubated with anti-BMP mAb or anti-IgG mAb for 30 min. It should be noted that long incubations with anti-BMP mAb can have deleterious effects on the physiology of late endosomes and disrupt endocytic trafficking (Chu et al., 2005; Kobayashi et al., 1999; Matsuo et al., 2004). The incubation time used in our assay was short to circumvent this issue. dfTAT was then added and cells were analyzed 1 h after incubation. Cytosolic penetration of dfTAT was abolished in the presence of anti-BMP mAb but unaffected by anti-IgG mAb (Fig. 4b and c). Moreover, anti-BMP mAb, but not anti-IgG mAb, also blocked the cytosolic penetration of macromolecules co-incubated with dfTAT (i.e. DEAC-k5 and Cre recombinase; Fig. S5). Notably, incubation with the antibody did not significantly impact the level of peptide internalized by endocytosis (as measured by flow cytometry and fluorescence of cell lysates). In addition, dfTAT co-localized with rab7-EGFP in cells incubated with anti-BMP mAb, indicating that the antibody treatment does not dramatically interfere with trafficking of dfTAT to late endosomes. Together, these results show that anti-BMP mAb blocks the endosomal leakage mediated by dfTAT, and, in doing so, inhibits the cytosolic penetration of both this delivery agent and its co-incubated cargos. Inhibition by anti-BMP is achieved without preventing dfTAT from accumulating into late endosomes. Overall, given the specific localization of BMP within the endocytic pathway (late endosomes and lysosomes) (Piper and Katzmann, 2007) and given that lysosomes were previously excluded as sites of

leakage, these experiments confirm the involvement of late endosomes in dfTAT-mediated cytosolic delivery and identify BMP as a cellular factor involved in endosomal escape. Based on our results, we propose that dfTAT escapes from endosomes and delivers macromolecules into the cytosolic space by mediating leaky-fusion: dfTAT binds lipid bilayers containing BMP, it promotes the fusion of vesicles containing BMP, and the fusion of these vesicles leads to leakage and delivery of cargos. It is in this context that anti-BMP exhibits its inhibitory effect: anti-BMP binds the surface of BMP-containing vesicles and prevents these vesicles from coming into contact with one another. Therefore, despite the fact that dfTAT might bind the surface of these vesicles, dfTAT-mediated leakage cannot take place because vesicle contact/fusion cannot proceed. A model for the cytosolic penetration of dfTAT is provided in Figure 5.

Discussion

Arginine-rich CPPs such as dfTAT can interact promiscuously with a number of negatively-charged species. On the cell surface, for instance, CPPs interact with heparan sulfate proteoglycans and this is thought to play a role in endocytic uptake (Nakase et al., 2006; Poon and Gariepy, 2007; Tyagi et al., 2001). Several models involving negatively-charged lipids have also been proposed to explain the direct plasma membrane translocation observed with certain CPPs (Ciobanasu et al., 2009; Katayama et al., 2013; Nakase et al., 2008). In the case of dfTAT, our data suggest that the late endosome lipid BMP is a primary mediator of cytosolic penetration. Based on the lipid composition of cellular membranes, BMP might be one of few anionic species that can come in direct contact with a compound trafficking through the endocytic pathway. For instance, other negatively-charged lipids such as phosphatidylserine are typically restricted to cytoplasmic leaflets (Leventis and Grinstein, 2010). Our data suggest that dfTAT transport to late endosomes is critical for endosomal escape and that increasing the concentration of peptide in the incubation media increases the likelihood that a threshold concentration will be reached within these organelles. Without excluding potential participation of other cellular factors, our *in vitro* experiments suggest that interactions with BMP may be sufficient to mediate the endosomal leakage activity of dfTAT. BMP can bind dfTAT and mediate its transfer into a hydrophobic environment. The molecular details of the interactions between these two species remain undefined. The differences observed between BMP and its structural isomer PG in the leakage and partitioning assays suggest that the negative charge of the lipids is required for recruitment of dfTAT to a lipid bilayer but that binding alone is not sufficient for leakage. Instead, the micellar/fusogenic propensities of BMP are important. Our *in vitro* fusion experiment suggests that, after binding of dfTAT to BMP, dfTAT can cause fusion of vesicles. This in turn, causes efficient leakage of molecules from vesicles (as shown in the *in vitro* leakage experiments of Figure 3). Overall, the outcome of dfTAT interaction with a BMP containing lipid bilayer is membrane leakage. This is mirrored *in cellulo*, as anti-BMP mAb inhibits dfTAT-induced endosomal leakage, presumably by blocking fusion events and subsequent membrane permeation. dfTAT-mediated fusion of vesicles is an essential step involved in cell penetration but, ultimately, it is dfTAT-mediated membrane leakage what is required to achieve translocation across the membrane of late endosomes. The translocation of dfTAT and of delivered macromolecules might take place at the limiting membrane of late

endosomes during fusion events with intraluminal vesicles (Figure 5). In this model, cytosolic access is concomitant with the fusion event. It is also possible that translocation first takes place during fusion events between intraluminal vesicles. Under this scenario, dfTAT and delivered macromolecules reach the cytosolic space by back fusion, an endogenous process in late endosomes (Le Blanc et al., 2005). Both models are non-mutually exclusive. We are currently performing electron microscopy experiments to shed light on these processes.

The differences observed between dfTAT and fTAT *in vitro* are consistent with the results observed *in cellulo*: unlike dfTAT, fTAT does not escape late endosomes efficiently and it does not mediate the leakage of L.E. LUVs. Given the structural similarities between fTAT and dfTAT, the dramatic difference in activity between these two compounds is surprising. A possible conclusion is that the two copies of fTAT present in dfTAT act in synergy. Understanding this synergy might, in turn, inform the design of optimally active cell delivery agents. While deciphering the basis for this synergy will be the focus of future studies, our partitioning data already highlight a possible mechanistic insight. BMP is capable of transferring dfTAT into a milieu of low dielectric constant at a much lower concentration than that required for a similar transfer of fTAT. This phenomenon is unexpected as the affinity of both dfTAT and fTAT for BMP-containing bilayers is relatively similar. In addition, considering that phase transfer presumably requires the shielding of the positively-charged peptides by the anionic BMP counter ion, one would expect an opposite effect as dfTAT has twice the number of charges present in fTAT, and therefore should require twice as much BMP for neutralization. This behavior is therefore currently puzzling. Admittedly, it is also unclear whether (or how) it relates to the endosomal leakage observed in cells. Yet, it is tempting to postulate that dfTAT causes efficient endosomal leakage because it can disrupt BMP bilayers at a lipid:peptide ratio significantly lower than that required for fTAT. Interestingly, others have previously postulated that BMP may act in concert with TAT monomer to cause membrane leakage (Yang et al., 2010). This idea, based on the notion that a positively charged CPP might interact with a negatively charged lipid present in the endocytic pathway, was substantiated by *in vitro* liposome leakage assays. Yet, given that the activity of TAT is relatively poor in cells, the involvement of BMP in the penetration activity of this CPP has not been established *in cellulo*. In this context, the work presented with dfTAT provides strong *in vitro* and *in cellulo* evidence that BMP is a cellular factor important for cell penetration. Moreover, dfTAT being an extremely active member of the CPP family, it is possible that the mechanistic insights identified herein also apply to less efficient CPPs.

As previously reported, dfTAT-mediated delivery is well tolerated by cells (i.e. low toxicity and undisturbed proliferation rates and transcriptional program), (Erazo-Oliveras et al., 2014). The results presented herein indicate that cytosolic penetration is, however, accompanied by the release of material trapped in the lumen of late endosomes. This presumably includes pro-apoptotic ions such as calcium and toxic proteins such as proteases. The leakage of such molecules into the cytosol of cells is known to trigger cell death, when endosomal membrane damage is mediated either photochemically or with lysosomotropic agents (Guicciardi et al., 2004; Muthukrishnan et al., 2012). For these reasons, lysosomes are often referred as the ‘suicide bags’ of the cells and similar potential toxic effects are also

often attributed to late endosomes. However, our data challenge the paradigm that efficient leakage cannot be achieved without toxic effects. A possible explanation might be related to the kinetics of endosomal leakage. For instance, dfTAT promotes an efficient yet relatively slow and progressive leakage. This is coupled to the maturation time required to achieve accumulation of the peptide in late endosomes and might, in turn, permit cells to eliminate toxic ions and proteins and maintain a homeostatic balance.

Overall, our results illustrate how the chemistry of late endosomes is exploited by dfTAT. The identification of the BMP/dfTAT interaction reveals a novel system involved in endocytic egress and cytosolic access that may provide a fundamental basis for the guided development of future delivery agents that can escape the endocytic pathway without excessive cellular damage.

Materials and Methods

Peptide design, synthesis and purification

All peptides were synthesized in-house by solid-phase peptide synthesis (SPPS) using standard Fmoc protocols. The crude peptide products were analyzed and purified by reverse-phase HPLC. The correct identity of the peptides was confirmed by MALDI-TOF. Detailed protocols are reported in the Supplemental Information section.

Delivery experiments

Cells were seeded and grown to 80–90 % confluency after 48 h. Each well was washed with PBS and with Leibovitz's L-15 medium (L-15). Cells were then incubated with peptide (using a specified concentration) or co-incubated with peptide and cargo (in the case of FITC-Tf) at 37 °C for 1 h or a specified time in L-15 (or L-15 lacking cysteine to avoid dfTAT reduction; no differences were however observed). Incubations were performed in the absence of serum in the media as BSA was previously found to inhibit dfTAT. Following peptide incubation, cells were washed with L-15 supplemented with heparin (L-15-H) (1 mg/mL). To establish cell viability, cells were incubated with L-15 supplemented with a SYTOX dye (5 μM, SYTOX Blue or SYTOX green, Invitrogen). SYTOX dyes stain only the DNA of cells with compromised plasma membranes (dead cells). Cells were placed on an inverted microscope (Model IX81, Olympus) equipped with a heating stage maintained at 37 °C a nd images were collected using a Rolera-MGI Plus back-illuminated electron-multiplying charge-coupled device (EMCCD) camera (Qimaging). The filter sets used are reported in the Supplemental Information section.

Cytosolic penetration was established qualitatively by 100X imaging and quantitatively by 20X imaging. Penetration (+) cells (cytosolic/nucleolar fluorescence distribution) were counted using the Slidebook and Image J softwares. Cells stained by a SYTOX dye were excluded from this analysis. The percentage of penetration (+) cells was calculated by dividing the nucleoli-positive cells by the total number of cells, obtained from bright field images. More than 500 cells were counted in each experiment from images obtained by scanning a well. Experiments were performed in triplicates.

For retrograde transport inhibition, cells were incubated with retro-2 (20 μM) for 30 min prior to incubation with dfTAT. Successful inhibition was tested by evaluating the effect of retro-2 on the transport of the TGN marker mEmerald-TGOLN2 (TGOLN2, also known as TGN38, cycles between the endocytic pathway, the TGN and the plasma membrane (Chia et al., 2011)). In order to address the involvement of lysosomes, cells were incubated with 50 μM DEAC-k5 for 1 h at 37 °C. Cells were washed three times with L-15-H. In one case, dfTAT, was incubated with cells immediately after washing the cells. In the other case, dfTAT was added 2 h after incubating the cells in L-15 at 37 °C. In each experiment, incubation with dfTAT was performed for 1 h at 37 °C. Cells were washed with L-15-H and LysoTracker® Green (500 nM) was added to stain acidic endocytic organelles. To establish the involvement of BMP *in cellulo*, cells were incubated with 50 μg/mL anti-BMP mAb (mouse, Z-PLBPA) or anti-IgG mAb (mouse, ab99763) for 30 min at 37 °C. Cells wer e washed with L-15-H and placed on the heating stage maintained at 37 °C. df TAT was incubated with cells for 1 h at 37 °C. Cells were washed with L-15-H. Im ages were acquired as described earlier.

For cellular co-localization experiments, the Manders' overlap coefficient R (measures how interdependent the red and green channels are) and colocalization coefficient M1 (measures the percentage of above-background pixels in the red channel that overlaps with above-background pixels in the green channel) were calculated using ImageJ (NIH).

Preparation of liposomes

Liposomes were prepared using DOPC, DOPE, BMP, DOPA, DOPG and cholesterol (Avanti Polar Lipids). Lipids in chloroform were transfer into a 20 mL scintillation vial at molar ratios of 77:19:4 BMP:PC:PE for intraluminal late endosome vesicles (L.E.), 96:4 PC:PE for L.E. vesicles without BMP (L.E. PC), 77:19:4 PA:PC:PE for L.E. vesicles where BMP was replaced with PA (L.E. PA), 77:19:4 PG:PC:PE for L.E. vesicles where BMP was replaced with PG (L.E. PG) and 65:15:20 PC:PE:Chol for early endosomes/plasma membrane vesicles (E.E./P.M.). Lipid films were prepared by evaporating the chloroform from the mixture utilizing a stream of N_2 and removing traces of the solvent *in vacuo*. The dry lipid films were hydrated with buffer containing 100 mM NaCl, 10 mM NaH_2PO_4 pH 5.5 (phosphate buffer) or 100 mM NaCl, 10 mM NaH_2PO_4 and 60 mM calcein when calcein was required. The solution was mixed by vortexing vigorously and was allowed to swell for 2 h at 42 °C under an atmosphere of N_2 to obtain MLVs. To obtain LUVs, MLVs were extruded (20 passes) through a 100 nm pore size polycarbonate membrane (Whatman) using a Mini-Extruder (Avanti Polar Lipids). The average diameter size distribution of the liposomes was determined by dynamic light scattering using a Zeta Sizer (Malvern instruments). The liposomes were stored at 4 °C under an atmosphe re of N_2 and used within two weeks of preparation. Liposomes loaded with calcein were separated from free calcein after extrusion by gel filtration using a Sephadex G-50 (GE Healthcare) column (2.5 × 17.5 cm). Fractions were collected in a 96-well plate and the absorbance at 450 nm and 750 nm was determined to identify fractions containing calcein and liposomes, respectively.

dfTAT-mediated disruption of liposomes

A calcein-leakage assay was employed to evaluate the permeabilization of liposomes by dfTAT. For this assay, LUVs of different lipid compositions containing 60 mM calcein in their lumen were prepared. LUVs were mixed with dfTAT and fTAT at different peptide:lipid ratios in phosphate buffer (100 mM NaCl, 10 mM NaH_2PO_4 pH 5.5). After 60 min, the amount of free calcein was established by purifying the supernatants obtained using an illustra NAP-10 Sephadex G-25 column (GE Healthcare). The supernatants obtained after low speed centrifugation were purified to exclude soluble liposomes. The fluorescence from free calcein, from the fractions collected, was measured using the blue channel (Ex 490 nm, Em 520–560 nm) of a Promega GloMax-Multi plate reader (Promega). The extent of liposomal lumen content release or % leakage was determined according to the following equation:

$$\%\text{Leakage}=100\times\frac{\text{Fl}_\text{t}-\text{Fl}_0}{\text{Fl}_\text{max}-\text{Fl}_0}$$

Where Fl_t is the free calcein fluorescence intensity of a sample at a specific peptide:lipid ratio measured after 60 min, Fl_0 is the free calcein fluorescence intensity of a untreated sample and Fl_{max} is the free calcein fluorescence intensity of a sample after treatment with 0.2 % Triton X-100.

Binding of dfTAT to liposomes

Ultracentrifugation was used to evaluate the affinity of dfTAT for lipid bilayers. For this assay, MLVs of different lipid compositions were used (MLVs sediment more readily than LUVs). MLVs were mixed with dfTAT at different peptide:lipid ratios in phosphate buffer (100 mM NaCl, 10 mM NaH_2PO_4 pH 5.5). After 10 min, the sample was centrifuged at 87,000 rpm (rotor radius: r_{min} = 30.0 mm r_{av} = 34.5 mm; r_{max} = 38.9). The amount of unbound peptide (P) was determined by measuring the TMR fluorescence intensity from the supernatant, after reduction with TCEP, using the red channel (Ex = 525 nm, Em = 580–640 nm) of a Promega GloMax-Multi plate reader (Promega). The extent of peptide binding was established according to the following equation:

$$P_b=P_\text{tot}-P$$

Where P_{total} is the amount of peptide from the supernatant in the absence of MLVs, P is the fraction of unbound peptide at a particular lipid concentration and P_b is the fraction of bound peptide at a particular lipid concentration.

Partitioning of dfTAT between hexanes and aqueous solution

A two-phase partitioning assay was used to evaluate the interactions between dfTAT and lipids. Dry lipids were dissolved in hexanes at varying concentrations. The lipid solution (100 μL) was added to the solution containing the peptide in phosphate buffer (100 mM NaCl, 10 mM NaH_2PO_4 pH 5.5). The solutions were mixed vigorously using a vortex mixer for 30 s and allowed to equilibrate for 30 min. To establish the amount of peptide remaining

in the aqueous phase, the TMR fluorescence intensity from the aqueous phase was measured. The aqueous phase (80 μL) was transferred to a 96-well plate containing 80 μL of 100 mM TCEP in phosphate buffer and mixed for 30 min using a nutator. The TMR fluorescence intensity was measured using the red channel (Ex = 525 nm, Em = 580–640 nm) of a Promega GloMax-Multi plate reader (Promega). The extent of peptide partitioning was established by dividing the fluorescence intensity obtained from the aqueous phase at a particular lipid concentration by the TMR fluorescence intensity from the aqueous phase obtained in the absence of lipids.

Supplementary Material

Refer to Web version on PubMed Central for supplementary material.

Acknowledgments

This article was supported by Award Number R01GM110137. We are grateful to professors Thomas Meek (Texas A&M University), Craig Kaplan (Texas A&M University) and Steve Lockless (Texas A&M University) for helpful comments about the manuscript. We thank Dr. Mauricio Lasagna for technical assistance with fluorescence fluorimeter and lipid mixing assay. We thank Michael Davidson (Florida State University) for mEmerald-TGNP-N-10, Gia Voeltz (University of Colorado) for GFP-rab5B, Sergio Grinstein (University of Toronto and The Hospital for Sick Children Research Institute) for GFP-rab5DN(S34N) and Richard Pagano (Mayo Clinic) for GFP-rab7 WT and GFP-rab7 DN.

References

Angeles-Boza AM, Erazo-Oliveras A, Lee YJ, Pellois JP. Generation of endosomolytic reagents by branching of cell-penetrating peptides: tools for the delivery of bioactive compounds to live cells in cis or trans. Bioconjug Chem. 2010; 21:2164–2167. [PubMed: 21043514]

Bechara C, Sagan S. Cell-penetrating peptides: 20 years later, where do we stand? FEBS Letters. 2013; 587:1693–1702. [PubMed: 23669356]

Bucci C, Lütcke A, Steele-Mortimer O, Olkkonen VM, Dupree P, Chiariello M, Bruni CB, Simons K, Zerial M. Co-operative regulation of endocytosis by three RAB5 isoforms. FEBS Letters. 1995; 366:65–71. [PubMed: 7789520]

Bucci C, Parton RG, Mather IH, Stunnenberg H, Simons K, Hoflack B, Zerial M, van der Sluijs P, Hull M, Webster P, et al. The small GTPase rab5 functions as a regulatory factor in the early endocytic pathway. Trends in Cell Biology. 2:361.

Bucci C, Thomsen P, Nicoziani P, McCarthy J, van Deurs B. Rab7: A Key to Lysosome Biogenesis. Molecular Biology of the Cell. 2000; 11:467–480. [PubMed: 10679007]

Chevallier J, Chamoun Z, Jiang G, Prestwich G, Sakai N, Matile S, Parton RG, Gruenberg J. Lysobisphosphatidic Acid Controls Endosomal Cholesterol Levels. Journal of Biological Chemistry. 2008; 283:27871–27880. [PubMed: 18644787]

Chia PZC, Gasnereau I, Lieu ZZ, Gleeson PA. Rab9-dependent retrograde transport and endosomal sorting of the endopeptidase furin. Journal of Cell Science. 2011; 124:2401–2413. [PubMed: 21693586]

Chu Z, Witte DP, Qi X. Saposin C–LBPA interaction in late-endosomes/lysosomes. Experimental Cell Research. 2005; 303:300–307. [PubMed: 15652344]

Ciobanasu C, Harms E, Tünnemann G, Cardoso MC, Kubitscheck U. Cell-Penetrating HIV1 TAT Peptides Float on Model Lipid Bilayers. Biochemistry. 2009; 48:4728–4737. [PubMed: 19400584]

Colpitts TM, Moore AC, Kolokoltsov AA, Davey RA. Venezuelan equine encephalitis virus infection of mosquito cells requires acidification as well as mosquito homologs of the endocytic proteins Rab5 and Rab7. Virology. 2007; 369:78–91. [PubMed: 17707875]

Dietz GPH, Bδhr M. Delivery of bioactive molecules into the cell: the Trojan horse approach. Molecular and Cellular Neuroscience. 2004; 27:85–131. [PubMed: 15485768]

Eguchi A, Meade BR, Chang Y-C, Fredrickson CT, Willert K, Puri N, Dowdy SF. Efficient siRNA delivery into primary cells by a peptide transduction domain-dsRNA binding domain fusion protein. Nat Biotech. 2009; 27:567–571.

El-Sayed A, Futaki S, Harashima H. Delivery of Macromolecules Using Arginine-Rich Cell-Penetrating Peptides: Ways to Overcome Endosomal Entrapment. AAPS J. 2009; 11:13–22. [PubMed: 19125334]

Erazo-Oliveras A, Muthukrishnan N, Baker R, Wang TY, Pellois JP. Improving the Endosomal Escape of Cell-Penetrating Peptides and Their Cargos: Strategies and Challenges. Pharmaceuticals. 2012; 5:1177–1209. [PubMed: 24223492]

Erazo-Oliveras A, Najjar K, Dayani L, Wang T-Y, Johnson GA, Pellois J-P. Protein delivery into live cells by incubation with an endosomolytic agent. Nat Meth. 2014; 11:861–867.

Feng, Y.; Press, B.; Chen, W.; Zimmerman, J.; Wandinger-Ness, A. [19] Expression and properties of Rab7 in endosome function. In: C.J.D.A.H. W.E. Balch. , editor. Methods in Enzymology. Academic Press; 2001. p. 175-187.

Gao S, Simon MJ, Morrison B Iii, Banta S. Bifunctional chimeric fusion proteins engineered for DNA delivery: Optimization of the protein to DNA ratio. Biochimica et Biophysica Acta (BBA) - General Subjects. 2009; 1790:198–207. [PubMed: 19402206]

Gilleron J, Querbes W, Zeigerer A, Borodovsky A, Marsico G, Schubert U, Manygoats K, Seifert S, Andree C, Stoter M, et al. Image-based analysis of lipid nanoparticle-mediated siRNA delivery, intracellular trafficking and endosomal escape. Nat Biotech. 2013; 31:638–646.

Gillmeister MP, Betenbaugh MJ, Fishman PS. Cellular Trafficking and Photochemical Internalization of Cell Penetrating Peptide Linked Cargo Proteins: A Dual Fluorescent Labeling Study. Bioconjug Chem. 2011; 22:556–566. [PubMed: 21405111]

Gruenberg J. The endocytic pathway: a mosaic of domains. Nat Rev Mol Cell Biol. 2001; 2:721–730. [PubMed: 11584299]

Guicciardi ME, Leist M, Gores GJ. Lysosomes in cell death. Oncogene. 2004; 23:2881–2890. [PubMed: 15077151]

Gujrati M, Malamas A, Shin T, Jin E, Sun Y, Lu Z-R. Multifunctional Cationic Lipid-Based Nanoparticles Facilitate Endosomal Escape and Reduction-Triggered Cytosolic siRNA Release. Molecular Pharmaceutics. 2014; 11:2734–2744. [PubMed: 25020033]

Hafez IM, Maurer N, Cullis PR. On the mechanism whereby cationic lipids promote intracellular delivery of polynucleic acids. Gene therapy. 2001; 8:1188–1196. [PubMed: 11509950]

Heitz F, Morris MC, Divita G. Twenty years of cell-penetrating peptides: from molecular mechanisms to therapeutics. British Journal of Pharmacology. 2009; 157:195–206. [PubMed: 19309362]

Herce HD, Garcia AE, Cardoso MC. Fundamental Molecular Mechanism for the Cellular Uptake of Guanidinium-Rich Molecules. Journal of the American Chemical Society. 2014; 136:17459–17467. [PubMed: 25405895]

Iversen T-G, Skotland T, Sandvig K. Endocytosis and intracellular transport of nanoparticles: Present knowledge and need for future studies. Nano Today. 2011; 6:176–185.

Katayama S, Nakase I, Yano Y, Murayama T, Nakata Y, Matsuzaki K, Futaki S. Effects of pyrenebutyrate on the translocation of arginine-rich cell-penetrating peptides through artificial membranes: Recruiting peptides to the membranes, dissipating liquid-ordered phases, and inducing curvature. Biochimica et Biophysica Acta (BBA) - Biomembranes. 2013; 1828:2134–2142. [PubMed: 23711826]

Kobayashi T, Beuchat M-H, Chevallier J, Makino A, Mayran N, Escola J-M, Lebrand C, Cosson P, Kobayashi T, Gruenberg J. Separation and Characterization of Late Endosomal Membrane Domains. Journal of Biological Chemistry. 2002; 277:32157–32164. [PubMed: 12065580]

Kobayashi T, Beuchat M-H, Lindsay M, Frias S, Palmiter RD, Sakuraba H, Parton RG, Gruenberg J. Late endosomal membranes rich in lysobisphosphatidic acid regulate cholesterol transport. Nat Cell Biol. 1999; 1:113–118. [PubMed: 10559883]

Kobayashi T, Stang E, Fang KS, de Moerloose P, Parton RG, Gruenberg J. A lipid associated with the antiphospholipid syndrome regulates endosome structure and function. Nature. 1998; 392:193–197. [PubMed: 9515966]

Kobayashi T, Startchev K, Whitney Andrew J, Gruenberg J. Localization of Lysobisphosphatidic Acid-Rich Membrane Domains in Late Endosomes. Biological Chemistry. 2001; 382:483–485. [PubMed: 11347897]

Le Blanc I, Luyet P-P, Pons V, Ferguson C, Emans N, Petiot A, Mayran N, Demaurex N, Faure J, Sadoul R, et al. Endosome-to-cytosol transport of viral nucleocapsids. Nat Cell Biol. 2005; 7:653–664. [PubMed: 15951806]

Lee YJ, Datta S, Pellois JP. Real-time fluorescence detection of protein transduction into live cells. Journal of the American Chemical Society. 2008; 130:2398–2399. [PubMed: 18251482]

Lee YJ, Erazo-Oliveras A, Pellois JP. Delivery of macromolecules into live cells by simple co-incubation with a peptide. Chembiochem : a European journal of chemical biology. 2010; 11:325–330. [PubMed: 20029930]

Lengfeld J, Wang Q, Zohlman A, Salvarezza S, Morgan S, Ren J, Kato K, Rodriguez-Boulan E, Liu B. Protein kinase C δ regulates the release of collagen type I from vascular smooth muscle cells via regulation of Cdc42. Molecular Biology of the Cell. 2012; 23:1955–1963. [PubMed: 22456512]

Leventis PA, Grinstein S. The Distribution and Function of Phosphatidylserine in Cellular Membranes. Annual Review of Biophysics. 2010; 39:407–427.

Li G, Barbieri MA, Colombo MI, Stahl PD. Structural features of the GTP-binding defective Rab5 mutants required for their inhibitory activity on endocytosis. Journal of Biological Chemistry. 1994; 269:14631–14635. [PubMed: 8182071]

Lin C, Engbersen JFJ. Effect of chemical functionalities in poly(amido amine)s for non-viral gene transfection. Journal of Controlled Release. 2008; 132:267–272. [PubMed: 18655813]

Liu BR, Lo S-Y, Liu C-C, Chyan C-L, Huang Y-W, Aronstam RS, Lee H-J. Endocytic Trafficking of Nanoparticles Delivered by Cell-penetrating Peptides Comprised of Nona-arginine and a Penetration Accelerating Sequence. PLoS One. 2013; 8:e67100. [PubMed: 23840594]

Mainou BA, Dermody TS. Transport to Late Endosomes Is Required for Efficient Reovirus Infection. Journal of Virology. 2012; 86:8346–8358. [PubMed: 22674975]

Matsuo H, Chevallier J, Mayran N, Le Blanc I, Ferguson C, Fauré J, Blanc NS, Matile S, Dubochet J, Sadoul R, et al. Role of LBPA and Alix in Multivesicular Liposome Formation and Endosome Organization. Science. 2004; 303:531–534. [PubMed: 14739459]

Muthukrishnan N, Johnson GA, Lim J, Simanek EE, Pellois JP. TAT-mediated photochemical internalization results in cell killing by causing the release of calcium into the cytosol of cells. Biochimica et biophysica acta. 2012; 1820:1734–1743. [PubMed: 22771830]

Nakase I, Tadokoro A, Kawabata N, Takeuchi T, Katoh H, Hiramoto K, Negishi M, Nomizu M, Sugiura Y, Futaki S. Interaction of Arginine-Rich Peptides with Membrane-Associated Proteoglycans Is Crucial for Induction of Actin Organization and Macropinocytosis†. Biochemistry. 2006; 46:492–501. [PubMed: 17209559]

Nakase I, Takeuchi T, Tanaka G, Futaki S. Methodological and cellular aspects that govern the internalization mechanisms of arginine-rich cell-penetrating peptides. Advanced Drug Delivery Reviews. 2008; 60:598–607. [PubMed: 18045727]

Nelson CDS, Carney DW, Derdowski A, Lipovsky A, Gee GV, O'Hara B, Williard P, DiMaio D, Sello JK, Atwood WJ. A Retrograde Trafficking Inhibitor of Ricin and Shiga-Like Toxins Inhibits Infection of Cells by Human and Monkey Polyomaviruses. mBio. 2013; 4

Perche F, Torchilin VP. Recent Trends in Multifunctional Liposomal Nanocarriers for Enhanced Tumor Targeting. Journal of Drug Delivery. 2013; 2013:32.

Piper RC, Katzmann DJ. Biogenesis and Function of Multivesicular Bodies. Annual Review of Cell and Developmental Biology. 2007; 23:519–547.

Poon GM, Gariepy J. Cell-surface proteoglycans as molecular portals for cationic peptide and polymer entry into cells. Biochemical Society Transactions. 2007; 35:788–793. [PubMed: 17635149]

Schwarze SR, Hruska KA, Dowdy SF. Protein transduction: unrestricted delivery into all cells? Trends in Cell Biology. 2000; 10:290–295. [PubMed: 10856932]

Scott CC, Vacca F, Gruenberg J. Endosome maturation, transport and functions. Seminars in Cell & Developmental Biology. 2014; 31:2–10. [PubMed: 24709024]

Sönnichsen B, De Renzis S, Nielsen E, Rietdorf J, Zerial M. Distinct Membrane Domains on Endosomes in the Recycling Pathway Visualized by Multicolor Imaging of Rab4, Rab5, and Rab11. The Journal of Cell Biology. 2000; 149:901–914. [PubMed: 10811830]

Stechmann B, Bai S-K, Gobbo E, Lopez R, Merer G, Pinchard S, Panigai L, Tenza D, Raposo G, Beaumelle B, et al. Inhibition of Retrograde Transport Protects Mice from Lethal Ricin Challenge. Cell. 2010; 141:231–242. [PubMed: 20403321]

Stenmark H, Parton RG, Steele-Mortimer O, Lutcke A, Gruenberg J, Zerial M. Inhibition of rab5 GTPase activity stimulates membrane fusion in endocytosis. EMBO Journal. 1994; 13:1287–1296. [PubMed: 8137813]

Sugaya K, Seto S, Tsujimura K, Koide Y. Mobility of late endosomal and lysosomal markers on phagosomes analyzed by fluorescence recovery after photobleaching. Biochemical and Biophysical Research Communications. 2011; 410:371–375. [PubMed: 21683685]

Tyagi M, Rusnati M, Presta M, Giacca M. Internalization of HIV-1 Tat Requires Cell Surface Heparan Sulfate Proteoglycans. Journal of Biological Chemistry. 2001; 276:3254–3261. [PubMed: 11024024]

Ullrich O, Reinsch S, Urbé S, Zerial M, Parton RG. Rab11 regulates recycling through the pericentriolar recycling endosome. The Journal of Cell Biology. 1996; 135:913–924. [PubMed: 8922376]

Varkouhi AK, Scholte M, Storm G, Haisma HJ. Endosomal escape pathways for delivery of biologicals. Journal of Controlled Release. 2011; 151:220–228. [PubMed: 21078351]

Vitelli R, Santillo M, Lattero D, Chiariello M, Bifulco M, Bruni CB, Bucci C. Role of the Small GTPase RAB7 in the Late Endocytic Pathway. Journal of Biological Chemistry. 1997; 272:4391–4397. [PubMed: 9020161]

Vivès E, Brodin P, Lebleu B. A Truncated HIV-1 Tat Protein Basic Domain Rapidly Translocates through the Plasma Membrane and Accumulates in the Cell Nucleus. Journal of Biological Chemistry. 1997; 272:16010–16017. [PubMed: 9188504]

Vonderheit A, Helenius A. Rab7 Associates with Early Endosomes to Mediate Sorting and Transport of Semliki Forest Virus to Late Endosomes. PLoS Biol. 2005; 3:e233. [PubMed: 15954801]

Wilson JM, de Hoop M, Zorzi N, Toh B-H, Dotti CG, Parton RG. EEA1, a Tethering Protein of the Early Sorting Endosome, Shows a Polarized Distribution in Hippocampal Neurons, Epithelial Cells, and Fibroblasts. Molecular Biology of the Cell. 2000; 11:2657–2671. [PubMed: 10930461]

Yang S-T, Zaitseva E, Chernomordik LV, Melikov K. Cell-Penetrating Peptide Induces Leaky Fusion of Liposomes Containing Late Endosome-Specific Anionic Lipid. Biophysical Journal. 2010; 99:2525–2533. [PubMed: 20959093]

Zerial M, McBride H. Rab proteins as membrane organizers. Nat Rev Mol Cell Biol. 2001; 2:107–117. [PubMed: 11252952]

Highlights

- dfTAT cytosolic penetration requires trafficking to late endosomes
- dfTAT causes the fusion and leakage of membranes that contain BMP
- Anti-BMP inhibits dfTAT activity *in vitro* and *in cellulo*
- Cytosolic access of macromolecules is enabled by the dfTAT/BMP lock and key pair.

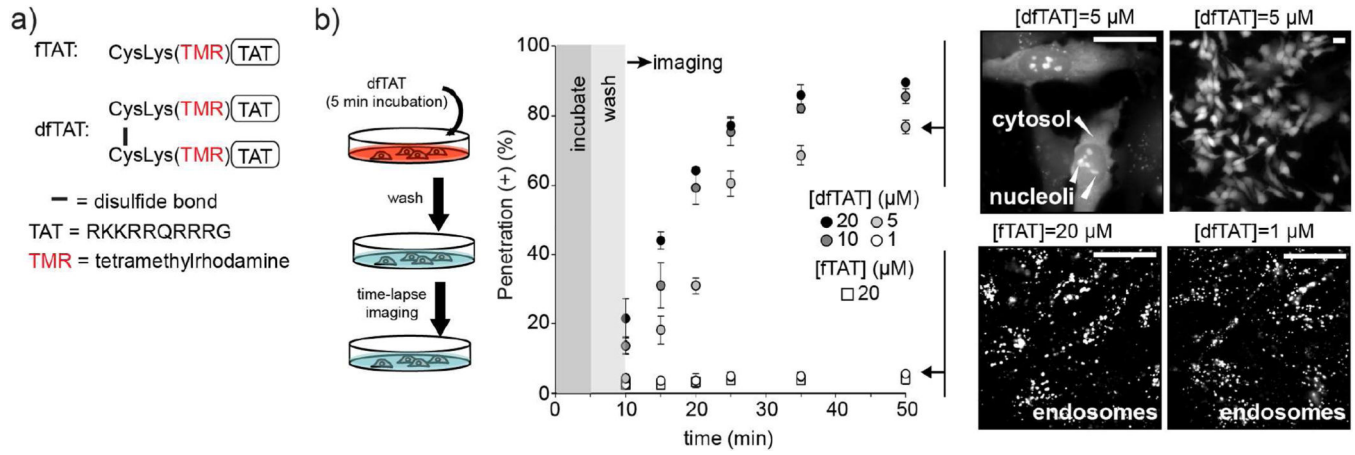

Figure 1.

dfTAT penetrates cells more efficiently than its monomeric counterpart fTAT. a) Peptide constructs. fTAT is a fluorescently-labeled analog of the prototypical CPP TAT. dfTAT is its disulfide bonded dimer (Erazo-Oliveras et al., 2014) b) Pulse chase experiment of cytosolic penetration. Cells are incubated with dfTAT at various concentrations (1, 5, 10 and 20 μM) for 5 min and washed with heparin to remove extracellular peptide. Fluorescence microscopy is then used to image cells at successive time points. Cells progress from a punctate fluorescence distribution to a cytosolic distribution when incubated with 5, 10, or 20 μM dfTAT. The fluorescence signal, presumably obtained from the reduced monomeric peptide after cytosolic access, also stains nucleoli. Cells incubated with 1 μM dfTAT or 20 μM fTAT display a punctate distribution throughout the experiment. Exclusion of the SYTOX Blue nuclear stain is used to confirm that the plasma membrane of the cells imaged is not compromised (not shown). The percentage of cells positive for cytosolic penetration, e.i. showing nucleoli staining while excluding SYTOX Blue, is reported as the mean of triplicate experiments for each conditions and the corresponding s.d. (>500 cells are imaged for each data point). Scale bars: 20 μm

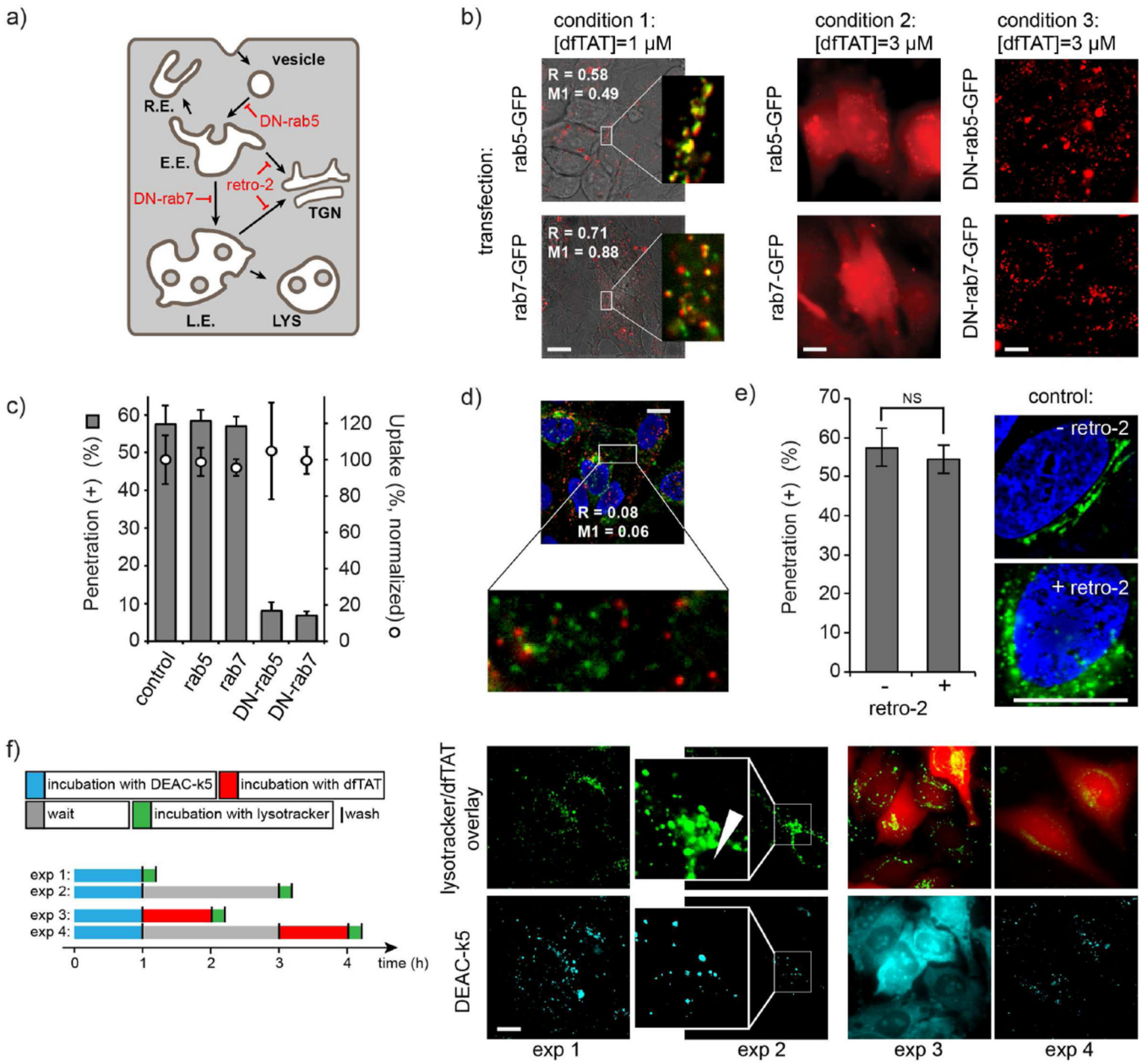

Figure 2.

dfTAT traffics through the endocytic pathway and penetrates the cytosolic space upon reaching late endosomes. a) Schematic representation of the endocytic pathway. Endocytic vesicle, early endosomes (E.E.), recycling endosomes (R.E.), late endosomes (L.E.) and lysosomes (LYS) are represented. Possible retrograde transport to the trans-Golgi network (TGN) is highlighted. b) At 1 μM (condition 1, [dfTAT] < threshold required for endosomal escape), dfTAT co-localizes with the E.E marker rab5-GFP and the L.E. marker rab7-EGFP (images are dfTAT/bright field overlays and inserts are dfTAT/GFP pseudocolored overlays; the Manders' overlap coefficient R and colocalization coefficient M1 are indicated). These markers do not block cytosolic penetration when dfTAT is incubated at 3 μM (condition 2, [dfTAT] > threshold required for endosomal escape) (images are dfTAT pseudocolored 100X

images). In contrast, dominant-negative rab5 and rab7 block cytosolic penetration and dfTAT (3 μM) remains trapped inside endosomes (condition 3). Scale bars: 20 μm. c) Quantitative measurements of the effect of rab5, rab7 and dominant negative mutants on cytosolic penetration and overall cellular uptake. dfTAT (3 μM) achieves cytosolic penetration in cells expressing rab5 and rab7. In contrast, DN-rab5 and DN-rab7 block cytosolic penetration without reducing overall endocytic uptake. Transfection efficiencies were established by monitoring EGFP fluorescence by flow cytometry (Fig. S3). d) dfTAT does not significantly co-localize with FITC-transferrin, a marker of recycling endosomes. Cell were co-incubated with dfTAT (1 μM) and FITC-transferrin (3 μg/mL) for 1 h, washed and imaged. The cell permeable nuclear stain DAPI was added during imaging. The image represented is a pseudocolored overlay where FITC-transferrin is green, dfTAT red, and DAPI blue. Scale bars: 20 μm e) The inhibitor of retrograde transport retro-2 does not impact the cytosolic penetration of dfTAT. No statistically significant difference (NS = P value>0.05, determined using a t-test analysis) in the number of penetration positive cells is observed when cells are incubated with dfTAT (3 μM, 1h incubation) with or without retro-2. Images represent a positive control experiment where retro-2 inhibits the transport of the Golgi marker mEmerald-TGOLN2. Images are overlay of DAPI (blue) and mEmerald-TGOLN2 (green). Upon treatment with retro-2, mEmerald-TGOLN2 loses its tubular localization and adopts a punctate distribution. Scale bars: 10 μm f) Cytosolic penetration does not involve leakage from lysosomes. Cells were incubated with DEAC-k5, a protease-resistant peptide labeled with a blue fluorophore. Staining with LysoTracker® Green, a marker of acidified endocytic organelles, shows entrapment of the peptide within the endocytic pathway. Overtime, DEAC-k5 accumulates in the perinuclear region, consistent with lysosomal accumulation (exp 2, white arrow shows the nucleus of the cell imaged). Incubation with dfTAT (5 μM, 1h) immediately after incubation with DEAC-k5 (50 μM, 1h) and washing cells leads to a distribution of both peptide in the cytosol and nuclei of cells (DEAC-k5 also displays a nucleolar staining). When dfTAT is incubated 2h after the incubation with DEAC-k5, dfTAT distribute throughout the cell but DEAC-k5 remains trapped inside perinuclear organelles. Scale bars: 20 μm. The data in c and e represent the mean of triplicate experiments and the corresponding s.d.

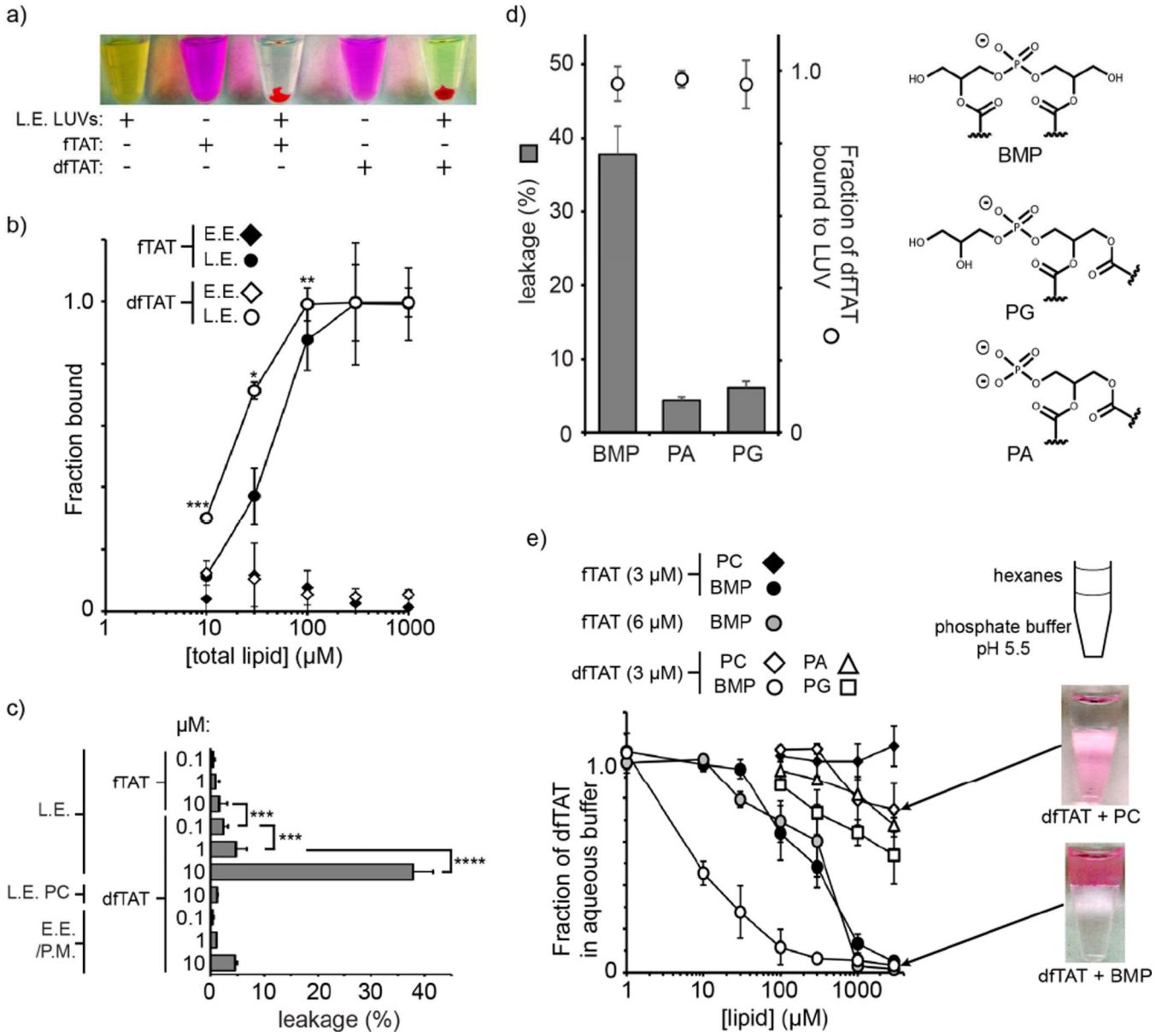

Figure 3.

dfTAT causes the leakage of liposomes of L.E. lipid composition by interacting with BMP. a) Representative images of a suspension of L.E. LUVs loaded with the green fluorophore calcein as an indicator of luminal leakage. Liposomes incubated with fTAT (10 μM) or dfTAT (10 μM) at a peptide:lipid ratio of 1:50 form aggregates containing both green and red fluorescence. The pellets obtained after low-speed centrifugation are shown. The supernatant is green (free calcein) after treatment with dfTAT but not after treatment with fTAT. P-values determined using t-test analysis are reported (*** = P≤0.001). b) Determination of the affinity of fTAT (3 μM) and dfTAT (3 μM) for multi-lamellar vesicles (MLVs) of E.E. or L.E. lipid composition. The fraction of peptide bound was determined by high-speed centrifugation of MLVs followed by quantification of the fluorescence signal remaining in the supernatant. P-values determined determined using t-test analysis between fTAT and

dfTAT at 10, 30 and 100 μM are reported (*= P ≤0.05, **= P ≤0.01, ***= P≤0.001). c) Quantification of the leakage activity of fTAT and dfTAT. Liposomes of E.E/P.M. or L.E. lipid composition were incubated with peptides as shown in A. Control LUVs containing PC in place of BMP where also used (L.E. PC). The fluorescence signal of calcein was quantified and compared to that obtained upon lysis of liposomes with the detergent Triton X (100% leakage control). d) Quantification of the leakage activity of dfTAT with LUVs containing the negatively-charged phospholipids BMP, PA, PG (polar heads are represented). LUVs (77:19:4 X:PC:PE where X is PA, PG, or BMP) were incubated with dfTAT (10 μM) to a final peptide:lipid ratio of 1:50. Leakage was quantified as in c) and the fraction of dfTAT bound to LUVs was quantified by measuring the fluorescence signal of TMR from the LUVs pellet formed after low-speed centrifugation. e) BMP-mediated partitioning of dfTAT into hexanes. dfTAT (3 μM) was incubated in phosphate buffer (pH 5.5) and the lipids PC, PA, PG or BMP dissolved in hexanes at various concentrations were added. The fraction of peptide that remains in the aqueous phase upon mixing was measured by fluorescence spectroscopy.

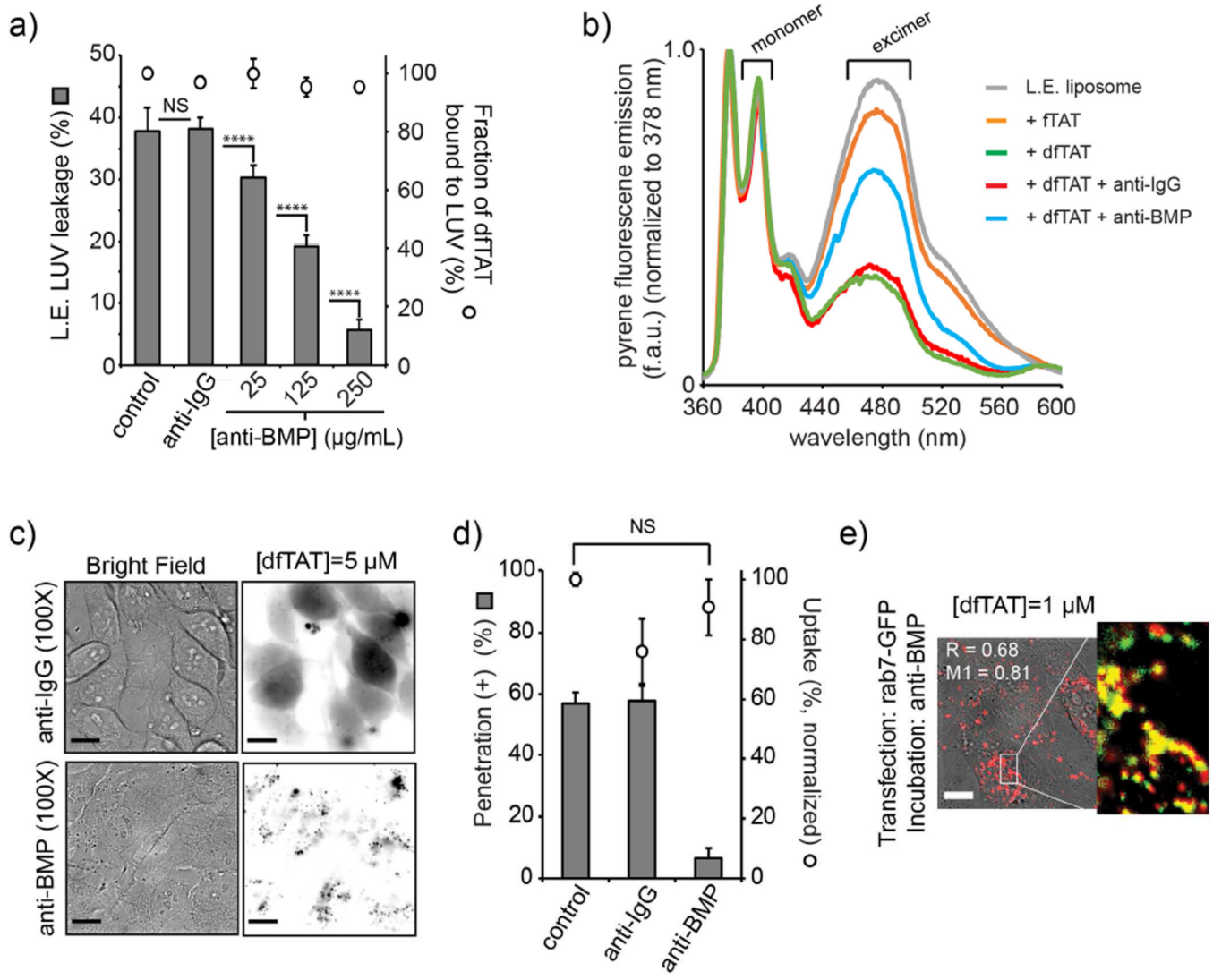

Figure 4.

The anti-BMP mAb inhibits cytosolic penetration. a) LUV leakage assay in the presence of anti-BMP mAb . Calcein leakage by dfTAT (10 μM) is measured as in Figure 3 (peptide:lipid ratio of 1:50). The presence of anti-BMP mAb (25, 125 and 250 μg/mL) or anti-IgG mAb (250 μg/mL) does not diminish the amount of peptide bound to LUVs, as measured by fluorescence spectroscopy of the pellet obtained after centrifugation. P-values determined using t-test analysis are reported (NS = P>0.05, **** = P≤0.0001). b) LUV lipid mixing assay in the presence of anti-BMP mAb. Lipid mixing between equal amounts of L.E. liposomes containing 10% pyrene-PC and unlabeled L.E. liposomes is measured by monitoring the decrease in excimer pyrene fluorescence. Pyrene fluorescence spectra were recorded 60 min after liposome mixing in the absence of peptide (L.E. liposome control), or in the presence of fTAT (10 μM) or dfTAT (10 μM) (peptide:lipid ratio of 1:50). Alternatively, LUVs were mixed and incubated with anti-IgG mAb or anti-BMP mAb (250 μg/mL) prior to peptide addition. A representative set of spectra from experiments performed in triplicate are reported. c) Incubation of cells with anti-BMP mAb abolishes the

endosomal escape of dfTAT. Cells were pre-incubated with anti-BMP mAb or the control anti-IgG mAb for 30 min. dfTAT (3 μM) was added in the presence of antibody (50 μg/mL) and imaging was performed after 1 h incubation. Scale bars: 20 μm d) Anti-BMP diminishes the cellular penetration activity of dfTAT without reducing how much peptide is endocytosed. Cytosolic penetration was scored as described in Figure 1. Total fluorescence of cell lysates was used to determine the effect of antibody incubation on the overall endocytic uptake of dfTAT. A T-test analysis indicates no statistically significant difference (NS= $P>0.05$) in the uptake of dfTAT in the absence or presence of anti-BMP. e) Anti-BMP does not prevent dfTAT from reaching late endosomes. A co-localization experiment of dfTAT (1 μM) with rab7-GFP was performed. After 1h incubation, dfTAT co-localizes with the L.E. marker rab7-EGFP in cells pre-treated with anti-BMP for 30 min (the image is a dfTAT/bright field overlay and the insert is a dfTAT/GFP pseudocolored overlay; the Manders' correlation overlap coefficient R (measures how interdependent the red and green channels are) and the Manders' colocalization coefficient M1 (measures the percentage of above-background pixels in the red channel that overlaps with above-background pixels in the green channel) are indicated. Scale bar: 20 μm

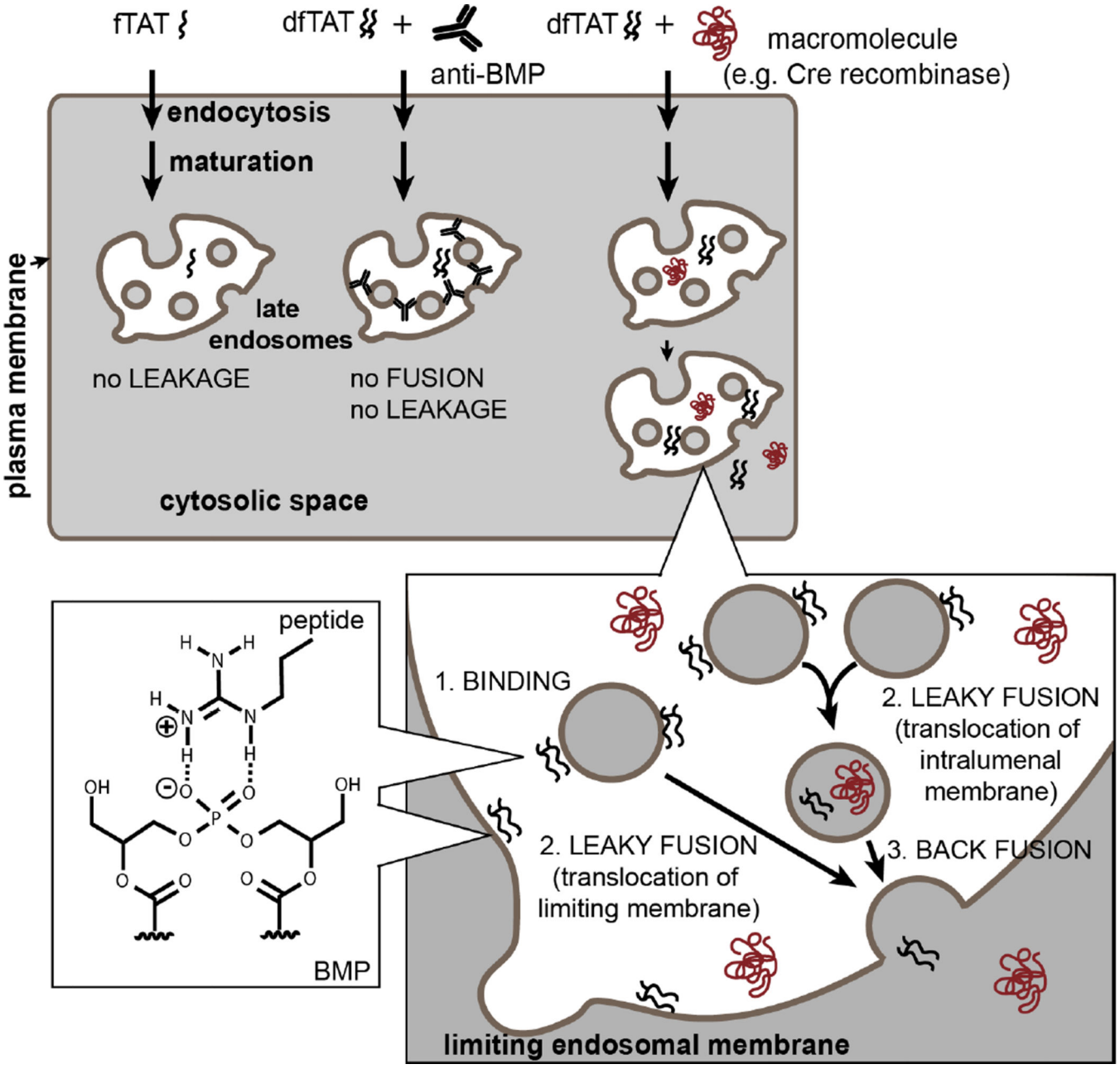

Figure 5.

Model of endosomal escape and cytosolic penetration by dfTAT. This illustration shows the accumulation of dfTAT into a late endosome after endocytosis and endocytic maturation. Late endosomes are drawn as membranous organelles containing intraluminal vesicles. The possible interaction between an arginine residue of dfTAT and the lipid BMP contained within the membranes of late endosomes is represented (the fatty acids of BMP are not drawn). Binding of dfTAT to other phospholipids on the cell surface or within the endocytic pathway is possible but the interaction with BMP preferentially results in membrane fusion and leakage. Inside late endosomes, dfTAT translocates into the cytosol by leaky-fusion events (two non-mutually exclusive scenarios involving intraluminal vesicles and the

limiting membrane of the organelle are represented). The membrane leakage induced by dfTAT during the leaky-fusion events also allow the translocation of macromolecules incubated and endocytosed with dfTAT. The inhibitory effect of anti-BMP mAb, which blocks fusion and subsequent leakage, is also highlighted.